The Great Oxidation Event preceded a Paleoproterozoic "snowball Earth"

Matthew R. Warke[a,1], Tommaso Di Rocco[a,b], Aubrey L. Zerkle[a,c], Aivo Lepland[d,e], Anthony R. Prave[a], Adam P. Martin[f,g], Yuichiro Ueno[h,i], Daniel J. Condon[f], and Mark W. Claire[a,c,j]

[a]School of Earth and Environmental Sciences, University of St Andrews, St Andrews KY16 9AL, Scotland, United Kingdom; [b]Geowissenschaftliches Zentrum, Universität Göttingen, 37077 Göttingen, Germany; [c]Centre for Exoplanet Science, University of St Andrews, St Andrews KY16 9AL, Scotland, United Kingdom; [d]Geological Survey of Norway, 7491 Trondheim, Norway; [e]Department of Geology, University of Tartu, 50441 Tartu, Estonia; [f]Natural Environment Research Council Isotope Geosciences Laboratory, British Geological Survey, Keyworth NG12 5GG, United Kingdom; [g]GNS Science, Dunedin, 9054, New Zealand; [h]Department of Earth and Planetary Sciences, Tokyo Institute of Technology, 152-8551 Meguro, Tokyo, Japan; [i]Earth-Life Science Institute, Tokyo Institute of Technology, Meguro, Tokyo 152-8550, Japan; and [j]Blue Marble Space Institute of Science, Seattle, WA 98154

Edited by Mark Thiemens, University of California San Diego, La Jolla, CA, and approved April 28, 2020 (received for review February 18, 2020)

The inability to resolve the exact temporal relationship between two pivotal events in Earth history, the Paleoproterozoic Great Oxidation Event (GOE) and the first "snowball Earth" global glaciation, has precluded assessing causality between changing atmospheric composition and ancient climate change. Here we present temporally resolved quadruple sulfur isotope measurements ($\delta^{34}S$, $\Delta^{33}S$, and $\Delta^{36}S$) from the Paleoproterozoic Seidorechka and Polisarka Sedimentary Formations on the Fennoscandian Shield, northwest Russia, that address this issue. Sulfides in the former preserve evidence of mass-independent fractionation of sulfur isotopes (S-MIF) falling within uncertainty of the Archean reference array with a $\Delta^{36}S/\Delta^{33}S$ slope of −1.8 and have small negative $\Delta^{33}S$ values, whereas in the latter mass-dependent fractionation of sulfur isotopes (S-MDF) is evident, with a $\Delta^{36}S/\Delta^{33}S$ slope of −8.8. These trends, combined with geochronological constraints, place the S-MIF/S-MDF transition, the key indicator of the GOE, between 2,501.5 ± 1.7 Ma and 2,434 ± 6.6 Ma. These are the tightest temporal and stratigraphic constraints yet for the S-MIF/S-MDF transition and show that its timing in Fennoscandia is consistent with the S-MIF/S-MDF transition in North America and South Africa. Further, the glacigenic part of the Polisarka Formation occurs 60 m above the sedimentary succession containing S-MDF signals. Hence, our findings confirm unambiguously that the S-MIF/S-MDF transition preceded the Paleoproterozoic snowball Earth. Resolution of this temporal relationship constrains cause-and-effect drivers of Earth's oxygenation, specifically ruling out conceptual models in which global glaciation precedes or causes the evolution of oxygenic photosynthesis.

quadruple sulfur isotopes | mass independent fractionation | Great Oxidation Event | snowball Earth

The early Paleoproterozoic transition from mass-independently fractionated sulfur isotopes (S-MIF) to mass-dependent fractionation (S-MDF; i.e., where $\Delta^{33}S$ and $\Delta^{36}S \approx 0$) is now recognized as a key proxy identifying a unidirectional and global rise in atmospheric oxygen (1), the Great Oxidation Event (GOE; ref. 2). In broad temporal proximity with the S-MIF/S-MDF transition were periods of severe glaciation, including at least one "snowball Earth" event (3, 4). However, assessing causality (if any) between, and enhancing understanding about, changing atmospheric chemistry and ancient climate change leading to glaciations is hindered by the poorly constrained timing of the S-MIF/S-MDF transition with respect to glacial deposits, a problem which is compounded by spurious intercratonic stratigraphic correlations (4–6). As a consequence, a variety of hypotheses, with disparate ordering of key Earth system events, have been advanced including planetary oxygenation being tied to secular changes in planetary degassing following an early evolution of oxygenic photosynthesis (7, 8), the evolution of oxygenic photosynthesis directly triggering a Paleoproterozoic snowball Earth glaciation (4), and/or chemical weathering following deglaciation leading to the GOE (9, 10). Additionally, complicating interpretations of the significance of the S-MIF/S-MDF transition is the "crustal memory effect" hypothesis (11), namely, the reduction in $\Delta^{33}S$ magnitude and prevalence of positive $\Delta^{33}S$ values in the early Paleoproterozoic could reflect oxidative weathering and erosion with subsequent incorporation of Archean S-MIF signals into younger sediments (11, 12). This has led some workers to suggest that the S-MIF/S-MDF transition in the rock record could lag the atmospheric transition by as much as 10 to 200 My (11, 13). Such a scenario undermines using the S-MIF/S-MDF transition as a chemostratigraphic correlation surface (14) and a unique time marker of planetary oxygenation (13, 15, 16), as well as obscuring causality between planetary oxygenation and glaciation (4, 9).

We present a temporally constrained $\Delta^{33}S$, $\Delta^{36}S$, and $\delta^{34}S$ dataset from the Seidorechka and Polisarka Sedimentary Formations of the Imandra/Varzuga Greenstone Belt in the northwest Russian portion (Kola Peninsula) of the Fennoscandian Shield (*SI Appendix*, Fig. S1). Our data enable us to constrain the nature of S-MIF recycling within the basin, determine the timing of the S-MIF/S-MDF transition, and confirm that the GOE preceded the Paleoproterozoic snowball Earth event.

Significance

The causality between the Paleoproterozic Great Oxidation Event (GOE) and a global "snowball Earth" glaciation has remained unresolved due to an inability to determine their relative timing. We present quadruple sulfur isotope data from northwest Russia which constrain the GOE between 2,501 and 2,434 Ma. These are the tightest temporal and stratigraphic constraints ever presented for the GOE and show that the GOE predates Paleoproterozic glaciation in Russia and snowball Earth deposits in South Africa. Our results preclude hypotheses of Earth's oxygenation in which global glaciation precedes or causes the evolution of oxygenic photosynthesis.

Author contributions: M.R.W., T.D.R., A.L.Z., A.L., A.R.P., A.P.M., D.J.C., and M.W.C. designed research; M.R.W., T.D.R., A.L.Z., and M.W.C. performed research; M.R.W., T.D.R., A.L.Z., Y.U., and M.W.C. contributed new reagents/analytic tools; M.R.W., T.D.R., A.L.Z., and M.W.C. analyzed data; M.R.W. wrote the paper; and T.D.R., A.L.Z., A.L., A.R.P., and M.W.C. contributed to writing the paper.

The authors declare no competing interest.

This article is a PNAS Direct Submission.

Data deposition: The data and methods supporting this article can be accessed on the University of St Andrews Research Portal (DOI: 10.17630/2faeb51f-7353-4fbc-abdd-cbc7991cf44b).

[1]To whom correspondence may be addressed. Email: mw438@st-andrews.ac.uk.

This article contains supporting information online at https://www.pnas.org/lookup/suppl/doi:10.1073/pnas.2003090117/-/DCSupplemental.

First published June 1, 2020.

Geological Setting and Chronological Constraints

The Imandra–Varzuga Greenstone Belt consists of a suite of Paleoproterozoic sedimentary and volcanic rocks that rest unconformably on a mostly Neoarchean gneissic basement (*SI Appendix*, Fig. S1). Key intervals of the succession were targeted for coring as part of the International Continental Scientific Drilling Program's Fennoscandian Arctic Russia - Drilling Early Earth Project (FAR-DEEP; ref. 17).

FAR-DEEP drillcore 1A recovered the Seidorechka Sedimentary Formation, a 120-m-thick succession of shallow-marine shale, siltstone, and minor limestone and sandstone that is divided into five lithostratigraphic members: Sandstone-Siltstone member, Dolostone member, Quartzite member, Limestone-Shale member, and Shale member (Fig. 1 and ref. 17). The formation overlies a pervasive zone of calcitization and sericitization developed on the underlying Kuksha Volcanic Formation that is interpreted as a paleoweathering crust (18). The Seidorechka Sedimentary Formation is overlain by the Seidorechka Volcanic Formation. Both the Kuksha and Seidorechka volcanic rocks are mostly basalts but contain minor dacitic and rhyolitic units.

The 129-m-thick Polisarka Sedimentary Formation was recovered in FAR-DEEP drillcore 3A and sharply overlies the Seidorechka Volcanic Formation. The Polisarka Sedimentary Formation is divided into a lower Limestone member and an upper glacigenic Greywacke-Diamictite member (17, 19); various basaltic, andesitic, and komatiitic lava flows and ultramafic intrusions punctuate the succession (Fig. 1). The Limestone member is comprised of rhythmic interlayers of shale, marl, and limestone interpreted as having been deposited in a low-energy subtidal setting (17). Dropstones have been reported in the Limestone member (17) but bedding-parallel foliation which flattens and rotates clasts renders this interpretation contestable (19). The formation is overlain by komatiitic lava flows of the Polisarka Volcanic Formation (Fig. 1 and ref. 17).

The maximum depositional age of the Imandra/Varzuga sedimentary succession is constrained by isotope dilution thermal ionization mass spectrometry (ID-TIMS) U-Pb zircon ages of 2,501.5 ± 1.7 Ma and 2,504.4 ± 1.5 Ma for the Neoarchean Pana Tundra and Monche plutons (20). The Seidorechka Volcanic Formation has a baddeleyite age of 2,442.2 ± 1.7 Ma and the spatially associated Imandra lopolith has a zircon age of 2,441 ± 1.6 Ma (both U-Pb ID-TIMS; ref. 20), whereas zircon grains from a metarhyodacite in the upper part of the formation are 2,448 ± 8 Ma in age (21). A 2,429 ± 6.6-Ma cross-cutting plagio-quartz dacitic metaporphyrite (U-Pb zircon SHRIMP; ref. 22) provides a minimum age for the Seidorechka Volcanic Formation. The Polisarka Volcanic Formation has yielded ID-TIMS zircon ages of 2,434 ± 6.6 Ma (19). Combined these constraints indicate that the Seidorechka Sedimentary Formation was deposited between 2,501.5 ± 1.7 Ma and 2,441 ± 1.6 Ma and the Polisarka Sedimentary Formation between 2,441 ± 1.6 Ma and 2,434 ± 6.6 Ma.

Results

Seidorechka Sedimentary Formation. Values of $\delta^{34}S$ range from −14.6 to +1.6‰ with a mean value of −6.8‰ (1σ = 3.8‰; $n = 24$) and show stratigraphic variation. Between ∼186 and ∼121 m, $\delta^{34}S$ values systematically increase upward (Fig. 1). Above 112 m (Shale member), $\delta^{34}S$ values are negative and do not show any stratigraphic trend. $\Delta^{33}S$ values vary from −0.43 to + 0.25‰ for the Seidorechka succession (*SI Appendix*, Table S1) but are almost entirely negative with a mean value of −0.14‰ (1σ = 0.14‰; $n = 24$). $\Delta^{36}S$ values range from −0.61 to 1.65‰ with a mean value of 0.16‰ (1σ = 0.52‰; $n = 23$).

Within the Seidorechka Sedimentary Formation there is no clear stratigraphic trend for $\Delta^{33}S$ values (Fig. 1). However, the Quartzite member has more negative and variable $\Delta^{33}S$ values (−0.43 to −0.29‰). $\Delta^{36}S$ values in the lower portion of the core are positive but above ∼140 m they become negative. $\Delta^{36}S$ values are highest in the Quartzite member and portions of the overlying Limestone-Shale member. There is a weak positive correlation between $\delta^{34}S$ and $\Delta^{33}S$ values in this formation (see Fig. 3).

Linear regression of a cross-plot of $\Delta^{33}S$ and $\Delta^{36}S$ values from the Seidorechka Sedimentary Formation yields a slope of −1.8 (Fig. 2*A*) but shallows to −1.6 if the Quartzite member is excluded. The calculation of $\Delta^{36}S/\Delta^{33}S$ slopes by linear regression ignores the abscissa's ($\Delta^{33}S$) uncertainty and cannot determine an uncertainty on the slope value itself; hence, we performed an orthogonal regression analysis, resulting in a $\Delta^{36}S/\Delta^{33}S$ slope of −1.86 ± 0.47 (1σ). Within uncertainty, the data fall along the "Archean reference array" (ARA; Fig. 2*B*). Mass-dependent fractionation processes can produce small-magnitude $\Delta^{33}S$ and $\Delta^{36}S$, which yield $\Delta^{36}S/\Delta^{33}S$ slopes ranging from −6 through −12 (23). Orthogonal regression analysis thus also allows us to state that the sulfur within the Seidorechka Sedimentary Formation demonstrates mass independence within an 8σ confidence interval.

Polisarka Sedimentary Formation. The Limestone member and Greywacke-Diamictite member archive distinctly different S isotope patterns (Figs. 1 and 2*A*). In the Limestone member, $\delta^{34}S$ values range from −26.6 to −10.2‰ (mean = −16.6‰; 1σ = 5.4‰; $n = 10$; *SI Appendix*, Table S2). Strongly negative $\delta^{34}S$ values are observed within a 14-m-thick interval (∼186 to 200 m) of limestone and shale. In contrast, in the diamictite $\delta^{34}S$ values range from −0.8 to 0.0‰ (mean = −0.5‰; 1σ = 0.3‰; $n = 5$). $\delta^{34}S$ values of the greywacke and dolarenite samples between ∼115 and ∼125 m transition from negative $\delta^{34}S$ values in the underlying Limestone member to near zero $\delta^{34}S$ values in the diamictite. Within this ∼10 m interval, $\delta^{34}S$ values increase from −8.5 to −1.6‰.

Within the majority of the Limestone member (depths > 170 m) $\Delta^{33}S$ values are low and positive, ranging from +0.03 to +0.05‰ (mean = +0.02; 1σ = 0.01‰; $n = 14$) and $\Delta^{36}S$ values are positive, ranging from +0.21 to +0.75‰ (mean = +0.45; 1σ = 0.16‰; $n = 14$). One dolarenite sample from the uppermost Limestone member (∼124 m) has a negative $\Delta^{33}S$ value of −0.38 that is similar to Seidorechka values.

Samples from the Limestone member (<170 m) plot tightly along a steep, mass-dependent $\Delta^{36}S/\Delta^{33}S$ slope of −8.8, as determined by the standard methodology of linear regression. (Fig. 2*A*). Orthogonal regression analysis including the analytical uncertainties in the $\Delta^{33}S$ predicts a much steeper slope of −61.7 ± 53.5 (1σ). While our data fit criteria in which best-fit orthogonal slopes are known to overpredict (*SI Appendix*, *Methods*), the analysis reveals that our data could be fit by a wide variety of slopes, including positive (as indicated by wide blue band in Fig. 2*C*). A distinctly mass-dependent slope of −8.2 is obtained as a one SD from the best orthogonal fit, complementing the slope of −8.8 from linear regression. The possibility remains that our Polisarka data were obtained from a distribution of samples with mass-independent properties, but we have demonstrated that such a sampling would have been a statistical aberration exceeding 1σ. We consider this possibility highly unlikely given that the consistently low $\Delta^{33}S$ values and expanded negative $\delta^{34}S$ range (Fig. 3) have the more parsimonious explanation of mass-conservation effects stemming from mass-dependent microbial processing (24).

Within the Greywacke-Diamictite member $\Delta^{36}S$ values are negative, ranging from −1.06 to −0.39‰ (mean = −0.60‰; 1σ = 0.59‰; $n = 5$) and $\Delta^{33}S$ values are low and consistently positive, ranging from +0.01 to +0.03‰ (mean = +0.02; 1σ = 0.01‰; $n = 14$). The $\Delta^{36}S/\Delta^{33}S$ values of the Greywacke-Diamictite member do not show any correlation but broadly cluster at the positive $\Delta^{33}S$ and negative $\Delta^{36}S$ range of values measured from the Seidorechka Sedimentary Formation and align the latter's $\Delta^{36}S/\Delta^{33}S$ slope (Fig. 2*A*). The dolarenite sample (∼124 m) of the

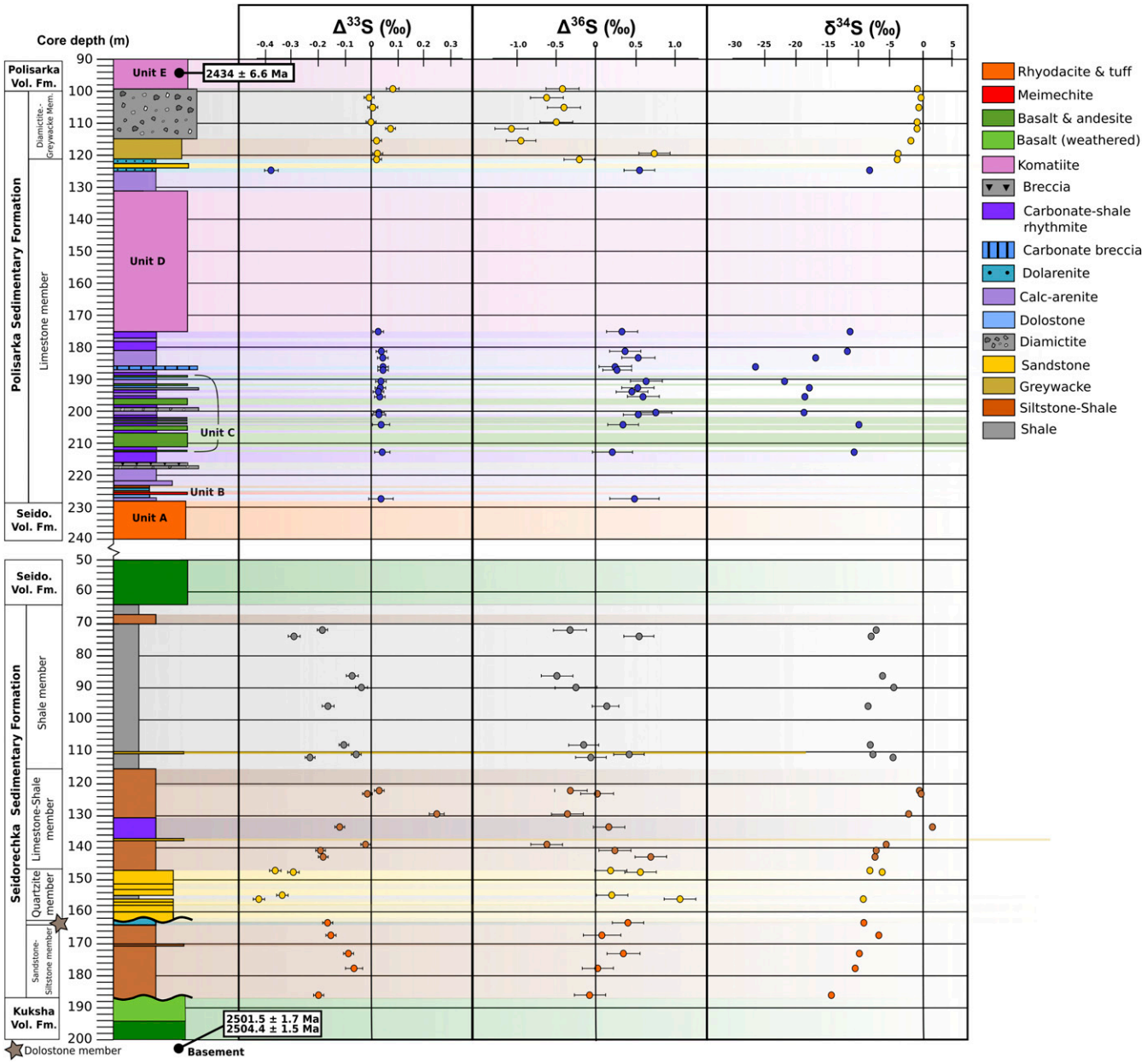

Fig. 1. Bulk rock-CRS $\Delta^{33}S$, $\Delta^{36}S$, and $\delta^{34}S$ measurements from the Seidorechka Sedimentary Formation (*Lower*) and Polisarka Sedimentary Formation (*Upper*). Core log summarized from previous studies (15, 17). Filled circle color corresponds to lithostratigraphic member: Seidorechka Sedimentary Formation: orange = Sandstone-Siltstone member, yellow = Quartzite member, brown = Limestone-Shale member, gray = Shale member; Polisarka Sedimentary Formation: dark blue = Limestone member, yellow = Diamictite-Greywacke member. Data point values and uncertainties are listed in *SI Appendix*, Tables S1 and S2; $\delta^{34}S$ error bars fall within the size of the symbol. Age dates that constrain the dataset are discussed in the text.

Limestone member plots in the negative $\Delta^{33}S$, positive $\Delta^{36}S$ quadrant and aligns strongly with the Seidorechka dataset (Fig. 2*A*). Polisarka samples fail to show any systematic correlation between the wide range of $\delta^{34}S$ values (~26‰) and the narrow range in $\Delta^{33}S$ values (<0.1‰; Fig. 3).

Discussion

Disappearance of S-MIF in Fennoscandia. Where $\Delta^{33}S$ carries a low-magnitude S-MIF signal, covariations in $\Delta^{36}S$ and $\Delta^{33}S$ are examined to ascertain whether an atmospheric S-MIF signature is preserved (25). Neoarchean and early Paleoproterozoic successions possess $\Delta^{36}S/\Delta^{33}S$ slopes of between −0.9 and −1.6 which define the ARA (26–30). Low-magnitude $\Delta^{36}S$ and $\Delta^{33}S$ values make calculation of $\Delta^{36}S/\Delta^{33}S$ slopes more uncertain (29). Our orthogonal regression analysis shows that the $\Delta^{36}S/\Delta^{33}S$ slope of the Seidorechka succession is consistent with the ARA (Fig. 3 *A* and *B*), indicating atmospheric production of S-MIF in the absence of ozone. In contrast, the steep $\Delta^{36}S/\Delta^{33}S$ slope of −8.8 for the Limestone member of the Polisarka Sedimentary Formation is inconsistent with the preservation of an atmospheric S-MIF signal (Fig. 2*A*). Whereas a positive relationship exists between $\Delta^{33}S$ vs. $\delta^{34}S$ in the Seidorechka Sedimentary Formation, in the Polisarka Sedimentary Formation very low $\Delta^{33}S$ values are associated with a wide scatter of negative $\delta^{34}S$ values (Fig. 4).

The near-zero $\Delta^{33}S$ values and $\Delta^{36}S/\Delta^{33}S$ characteristics of the Greywacke-Diamictite member, and a lone dolarenite sample from the Limestone member, fall within the $\Delta^{36}S/\Delta^{33}S$ slope typifying the Seidorechka succession (Figs. 2*A* and 3C). This

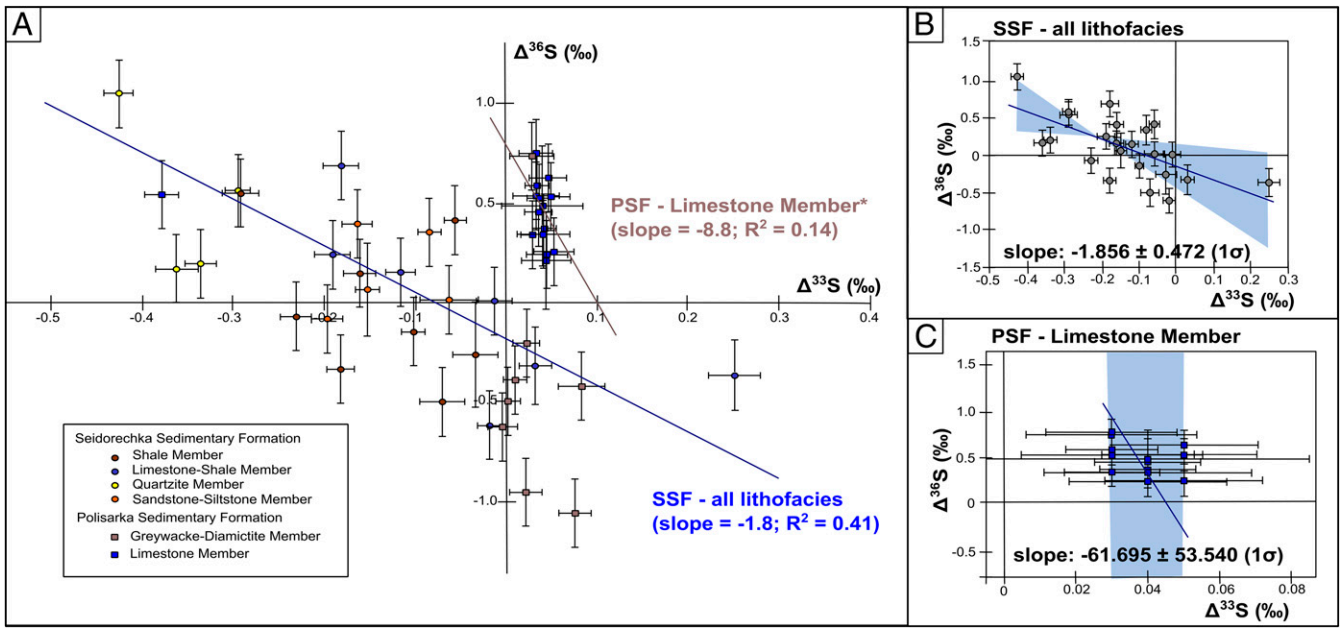

Fig. 2. (*A*) Cross-plot of $\Delta^{33}S$ and $\Delta^{36}S$ values from both the Polisarka (squares) and Seidorechka (circles) successions with marker color as assigned in Fig. 1 and shown in the key. Slope values were calculated using linear regression. Error bars are as listed in *SI Appendix*, Tables S1 and S2. (*B*) Orthogonal regression plot of all facies from the Seidorechka Sedimentary Formation (gray circles) showing calculated $\Delta^{36}S/\Delta^{33}S$ slope (blue line) and 3σ confidence interval (shaded blue area). (*C*) Orthogonal regression plot of the Limestone member (Polisarka Sedimentary Formation; dark blue squares) showing calculated $\Delta^{36}S/\Delta^{33}S$ slope (gray line) and 3σ confidence interval (shaded blue area).

apparent return of S-MIF coincides with facies that record increased detrital input by glacigenic and/or higher-energy processes (e.g., dolarenite). Critically, there is direct correspondence between S isotope values and lithofacies: the intervals of "normal" or "background" sedimentation do not show S-MIF, whereas those of enhanced sediment flux (e.g., diamictite) do. The most parsimonious interpretation of this pattern is that the enhanced flux obscured the S-MDF signal by bringing into the basin detritus carrying a recycled S-MIF signal.

Our findings are clear: the $\Delta^{36}S/\Delta^{33}S$ and $\Delta^{33}S/\delta^{34}S$ trends in the lower Polisarka Sedimentary Formation require that the S-MIF/S-MDF transition, often invoked as the key GOE indicator, occurred within a 70-My window bracketed by ∼2,501 Ma and ∼2,434 Ma. However, the duration was likely much less as three unconformities occur within that time window: 1) The basement-sediment contact is a major nonconformity marked by an erosive-based conglomerate unit comprised of basement-derived clasts, 2) a thick (as much as 10 m) paleoweathering crust separates the Seidorechka Sedimentary Formation from the underlying Kuksha volcanic rocks, and 3) the base of the quartzite unit in the middle of the Seidorechka Sedimentary Formation defines an angular unconformity. Further, the glacigenic diamictite and associated units of the Polisarka succession occur 60 m above sedimentary units containing S-MDF signals. This confirms that the S-MIF/S-MDF transition predates the glaciation but precludes a precise estimate of the time interval between disappearance of S-MIF and the glaciation.

It is not possible to test whether the S-MIF signal reappears above the diamictite as the glacial unit is overlain by Polisarka Volcanic Formation (Fig. 1). The volcanic units are in turn overlain by the Umba Sedimentary Formation but, as the latter preserves the Lomagundi–Jatuli positive carbonate isotope excursion, it likely dates to ∼2,200 to 2,060 Ma (17) and irreversible disappearance of the S-MIF signal has been demonstrated by this period (31).

Crustal Recycling of S-MIF Signals. The recurrence of S-MIF in the glacial Greywacke-Diamictite member implies that S-MIF recycling can temporarily overwhelm a background mass-dependent signal as highlighted by the "crustal memory effect" hypothesis. However, the near-zero $\Delta^{33}S$ values and S-MDF $\Delta^{36}S/\Delta^{33}S$ characteristics of the

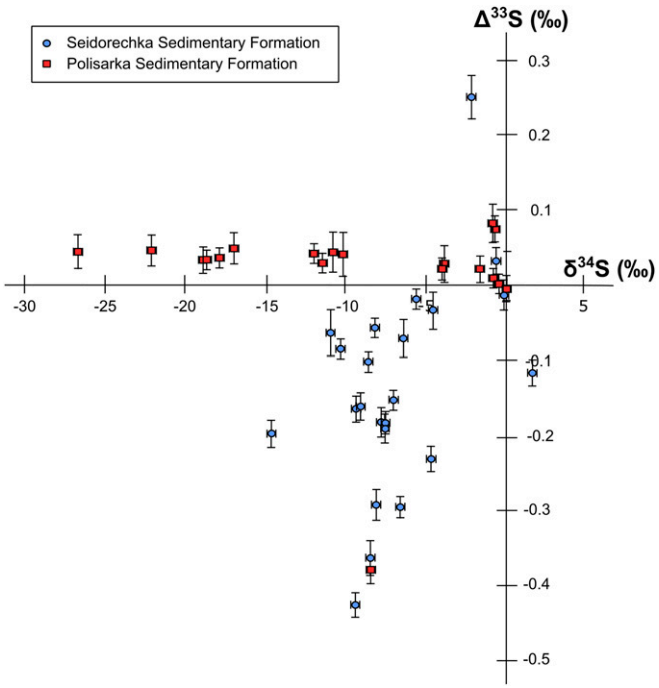

Fig. 3. Cross-plot of $\Delta^{33}S$ and $\delta^{34}S$ values from both the Polisarka (red squares) and Seidorechka (blue circles) successions. Error bars displayed are as listed in *SI Appendix*, Tables S1 and S2.

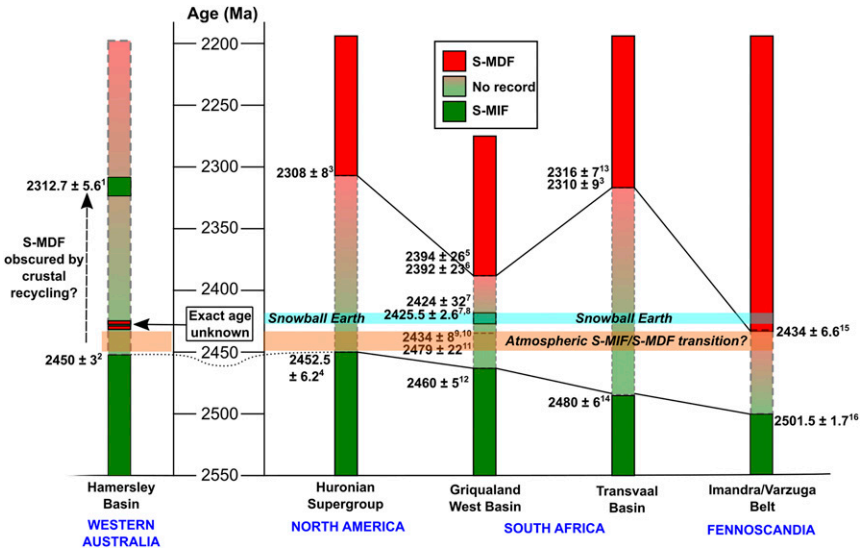

Fig. 4. Summary of the age constraints exerted on the timing of the S-MIF/S-MDF transition across Fennoscandia, South Africa, North America, and western Australia. Last known occurrences of S-MIF are shaded green and first known occurrences of S-MDF are shaded red, with intermediate faded shading between the two representing periods of nondeposition, undated strata, and strata with no multiple sulfur isotope record. The approximate position of the Makganyene snowball Earth deposit is shown as a blue band across the four cratons. The possible timing of the atmospheric S-MIF/S-MDF transition is shown as an orange band. Further details on age constraints, including references, are given in *SI Appendix*, Table S3.

lower Polisarka Sedimentary Formation are incompatible with that effect operating for a prolonged period (i.e., $>10^6$ to 10^7 years as predicted by end-member box models) after the atmospheric S-MIF/S-MDF transition (11, 13). The negative $\Delta^{33}S$ values in the Seidorechka Sedimentary Formation also rule out the possibility that the S-MIF/S-MDF transition (i.e., the GOE) occurred prior to 2.5 Ga and that the subsequent $\Delta^{33}S$ record is derived from crustal recycling of older S-MIF signals (15); crustal recycling, operating in this manner, would lead to solely positive $\Delta^{33}S$ values in the Paleoproterozoic (11). As such, the negative $\Delta^{33}S$ values from the Seidorechka Sedimentary Formation are more consistent with a coeval atmospheric signal. Negative $\Delta^{33}S$ values can be sustained through crustal recycling after the S-MIF/S-MDF transition but only for between 10^4 and 10^5 y (11), so even if sedimentary recycling (crustal memory effect) affected the Imandra–Varzuga rocks, the Seidorechka Sedimentary Formation would still only postdate the GOE by <1 My.

Crustal recycling of S-MIF signals was not continuous but was tied to periods of enhanced sediment input. This raises the possibility of variability in $\Delta^{33}S$ and $\Delta^{36}S$ values within, and between, Paleoproterozoic depositional basins as a function of changing patterns of sediment delivery, both spatial and temporal. Our results show that the atmospheric S-MIF/S-MDF transition can be rapidly and reliably recorded in the rock record. This raises the possibility that, eventually, it may prove suitable for demarcating the Archean–Proterozoic boundary, but only if further investigation continues to support that it is globally synchronous and unidirectional. Additionally, our results show that complementary assessment of sedimentological processes must be conducted to identify any potential spatially or temporally localized crustal recycling processes that may obscure the transition (13) and undermine its usefulness as a chronostratigraphic marker horizon (14).

Is the S-MIF/S-MDF Transition Globally Asynchronous? Constraining the precise timing of the S-MIF/S-MDF transition has been frustrated by a lack of robust absolute age constraints. However, improved stratigraphic correlations between western Australia, Fennoscandia, North America, and southern Africa have emerged (13, 16, 31–33). In the discussion below we summarize these and compare them to the constraints now established for Fennoscandia (Fig. 4).

The laterally correlative Duitschland and Rooihoogte Formations (Transvaal Basin, South Africa) archive the S-MIF/S-MDF transition (16, 34–36). The Duitschland Formation has an upper S-MDF–bearing portion and lower S-MIF–bearing portion that are separated by a major regional unconformity of unknown duration (36). The lower portion was deposited between 2,480 and 2,310 Ma (37, 38). The upper portion is younger than ∼2,424 Ma but could be closer to ∼2,310 Ma in age based on dating of the conformably overlying successions (31, 38, 39). Geochronological data for the Griqualand West Basin (Fig. 4) are sparse but the first appearance of a mass-dependent signal is in the Mooidraai Formation based on five samples that define a $\Delta^{36}S/\Delta^{33}S$ slope of −12 (34), implying that the S-MIF/S-MDF transition had occurred by ∼2,390 Ma (40, 41).

In western Australia, the S-MIF/S-MDF transition is ambiguous. In the Boolgeeda Iron Formation (Hamersley Group, western Australia) an S-MDF signal is first recorded after 2,450 Ma (13, 33), which is broadly coeval with the Fennoscandian S-MIF/S-MDF transition, but is succeeded by S-MIF signals. Siltstones at the top of the Boolgeeda Iron Formation contain pyrite with cores and rim compositions consistent with sulfate reduction of a sulfate reservoir with a recycled S-MIF component (13). Such values could be consistent with the crustal memory effect and could have occurred within 10^5 to 10^7 y of the S-MIF/S-MDF transition. However, other sulfur isotope studies of the Boolgeeda Iron Formation have contrasting $\Delta^{33}S$ and $\delta^{34}S$ values, including negative $\Delta^{33}S$ values that would be inconsistent with the crustal memory effect and indicative of a reducing atmosphere (42). In the overlying Turee Creek Group ($\leq$2,312 ± 22 Ma) two intervals record positive $\Delta^{33}S$ values and $\Delta^{36}S/\Delta^{33}S$ values that fall on the ARA (13). However, both intervals either consist of clastic and glacigenic sedimentary rocks or were deposited in an environment that experienced significant detrital input (43). Thus, the S-MIF signals recorded in both intervals could reflect similar, localized crustal recycling processes as previously inferred (13). Such overprinting likely reflects discrete periods of enhanced sediment influx, such as during periods of

deglaciation, rather than prolonged and continuous (10^8 y) operation of the crustal memory effect.

The S-MIF/S-MDF transition in the Huronian Supergroup on the Superior Craton (North America) is constrained to between the extrusion of the Copper Cliff Rhyolite at 2,452.5 ± 6.2 Ma and ∼2,308 Ma (Fig. 4 and refs. 31, 44, and 45), though this has been disputed (46). Given the thickness of strata and presence of major stratigraphic unconformities between the S-MIF-bearing Pecors Formation and S-MDF-bearing Espanola Formation, the S-MIF/S-MDF transition is likely considerably older than ∼2,308 Ma.

In summary, and notwithstanding the potential for enhanced sediment flux to mask the timing of the S-MIF/S-MDF transition, the current age constraints indicate that the transition is broadly synchronous across North America, South Africa, and Fennoscandia. The transition in western Australia remains uncertain and could be obscured by crustal recycling processes.

The GOE Preceded a Paleoproterozic Snowball Earth. In the Griqualand West Basin, the glacigenic Makganyene Formation is intercalated with the volcanic Ongeluk Formation, which was extruded in the low latitudes, suggesting the Makganyene glaciation may represent a Paleoproterozic snowball Earth event (3). The Ongeluk Formation, and associated feeder systems such as the Westerberg Sill Province and doleritic dyke swarms, date to 2,425.5 ± 2.6 Ma (16, 47). This age also constrains the snowball Earth event to before ∼2,428 to ∼2,423 Ma (Fig. 4).

This age corresponds within uncertainty to that of the diamictite-bearing Polisarka Sedimentary Formation in the Imandra/Varzuga Belt that, as shown above, shows that the S-MIF/S-MDF transition occurred prior to that glaciation. Although the paleolatitude of the Fennoscandian Shield is not known at this time, the geochronological constraints confirm that it is equivalent to the South African snowball Earth deposit. These combined results confirm that the GOE, as monitored by the S-MIF/S-MDF transition, preceded the Paleoproterozoic snowball Earth.

Our findings allow us to constrain some of the causalities that may exist between planetary oxygenation, the evolution of Earth's early greenhouse, and periods of severe glaciation (4, 6–10). In particular, our results resolve the long-standing issue of relative timing between these events and rules out conceptual models in which the evolution of oxygenic photosynthesis results from global glaciation. Given the lack of robust estimate of the time separating the disappearance of S-MIF and the glacial interval, our results do not explicitly rule out a model in which the evolution of oxygenic photosynthesis has a direct, nearly instantaneous causal effect on global glaciation (4). However, in the time since this conceptual model was published substantial evidence of oxygen production in aqueous Neoarchean and pre-GOE Paleoproterozoic environments has become apparent, necessitating an earlier evolution of oxygenic photosynthesis (48, 49). We make the explicit distinction here between proxies which point to localized oxygen production in aqueous environments and/or underneath microbial mats (but are sometimes described as constraining "atmospheric" oxygen), and the S-MIF proxy which unequivocally demands that the atmosphere was free from O_2/O_3. If oxygenic photosynthesis evolved early, as evidenced by many geochemical proxies, the S-MIF proxy demands that the Earth system must have strong sinks and feedbacks which kept the atmosphere reducing despite localized oxygen fluxes.

The presence of oxygen oasis in aqueous environments and underneath microbial mats is fully consistent with an overlying anoxic atmosphere given oxygen's extreme reactivity with the abundant and varied reducing atmospheric sinks such as hydrogen and methane (7, 50). Indeed, the paleoweathering crust developed on the Kuksha Volcanic Formation indicates rainwaters during this time contained no dissolved oxygen (18) along with evidence for enhanced CO_2 that would have contributed to the global greenhouse at that time. Given that a carbonate–silicate cycle buffering would likely have maintained climate on million-year timescales, some sort of "tipping point" is needed that would have affected global climate within a shorter amount of time. Our preferred explanation is that the tipping point likely involved the collapse of a methane greenhouse leading to both the disappearance of S-MIF along with a relatively rapid climate cooling. As a whole, our results and interpretations broadly support the "consensus" evolution of Earth's climate and atmospheric chemistry in the period leading up to the GOE (49, 51).

Conclusions

The Seidorechka Sedimentary Formation in Fennoscandia preserves small negative $\Delta^{33}S$ values and aligns along a $\Delta^{36}S/\Delta^{33}S$ slope that is consistent with the ARA and an atmospheric S-MIF signal. Overlying sediments from the Polisarka Sedimentary Formation preserve near-zero $\Delta^{33}S$ values and lie along a steep $\Delta^{36}S/\Delta^{33}S$ slope that is consistent with S-MDF. This observation constrains the timing of the S-MIF/S-MDF transition, and therefore the establishment of an oxidizing atmosphere on Earth, to between ∼2,501 and ∼2,434 Ma. Critically, this transition occurred sometime prior to the *ca*. 2,428- to 2,423-Ma snowball Earth glaciation given that the glacigenic part of the Polisarka Formation occurs ∼60 m above S-MDF–bearing strata of the Polisarka Sedimentary Formation. This is the tightest temporal constraint yet imposed on the GOE and the agreement between the Fennoscandian and South African sulfur isotope records shows that the S-MIF/S-MDF transition preceded a Paleoproterozoic snowball Earth event.

Methods

Samples and Protocol. FAR-DEEP drill-cores 1A and 3A were sampled using known procedures (52). Core samples (rock types listed in *SI Appendix*, Tables S1 and S2) were cut, crushed, and prepared for isotopic analysis using previous described techniques (29, 30) which are described fully in the *SI Appendix*. $\delta^{34}S$ values were measured on SO_2 gas at the University of St Andrews, Scotland, using a Thermo Isolink Elemental Analyzer coupled with a MAT 253 mass spectrometer in continuous-flow mode. The analytical uncertainty for $\delta^{34}S$ is better than 0.3‰ (1σ). Minor sulfur isotope analyses ($\delta^{33}S$, $\delta^{36}S$) were performed on SF_6 gas at the University of St Andrews using offline SF_6 generation and a second, dedicated Thermo MAT253 mass spectrometer in dual-inlet mode. SF_6 gas was generated by flash-heating Ag_2S to 590 °C in the presence of a solid fluorinating agent, CoF_3, using an updated Curie point pyrolysis method (53) detailed in *SI Appendix*. $\Delta^{33}S$ values were calculated as $\Delta^{33}S = 1{,}000 * [\ln((\delta^{33}S)/1{,}000 + 1) - 0.515 * \ln(\delta^{34}S)/1{,}000 + 1)]$ and $\Delta^{36}S$ values were calculated as $\Delta^{36}S = 1{,}000 * [\ln((\delta^{36}S)/1{,}000 + 1) - 1.9 * \ln(\delta^{34}S)/1{,}000 + 1)]$. Analytical uncertainty was determined from repeated analysis of IAEA-S1 between March 2019 and January 2020 ($n = 64$), yielding $\Delta^{33}S$ and $\Delta^{36}S$ values of 0.116 ± 0.015‰ and −0.572 ± 0.177‰ (mean ± 1σ), respectively. In addition to linear regression, orthogonal data regression (ODR) was used to incorporate uncertainties in both the abscissa and ordinate and quantifies the uncertainty in the determination of $\Delta^{36}S/\Delta^{33}S$ slopes.

Materials and Data Availability. All information pertaining to the experimental protocol and ODR analysis is fully detailed in *SI Appendix*. All raw isotope data and sample metadata are reported in *SI Appendix*, Tables S1 and S2, and all IAEA-S1 standard data are shown in *SI Appendix*, Fig. S2 and listed in full in Dataset S1. The data and methods supporting this article can be accessed on the University of St Andrews Research Portal (54).

ACKNOWLEDGMENTS. We thank M. Mesli for assistance during core sampling, Yanan Shen and an anonymous reviewer whose comments greatly improved the manuscript, and the St Andrews MIF In Atmospheres group for useful discussions. This project has received funding from the European Research Council under the European Union's Horizon 2020 research and innovation programme (Grant 678812 to M.W.C.).

1. J. Farquhar, H. Bao, M. Thiemens, Atmospheric influence of Earth's earliest sulfur cycle. *Science* **289**, 756–758 (2000).
2. H. D. Holland, The oxygenation of the atmosphere and oceans. *Philos. Trans. R. Soc.Lond. B Biol. Sci.* **361**, 903–915 (2006).
3. D. A. Evans, N. J. Beukes, J. L. Kirschvink, Low-latitude glaciation in the Palaeoproterozoic era. *Nature* **386**, 262–266 (1997).
4. R. E. Kopp, J. L. Kirschvink, I. A. Hilburn, C. Z. Nash, The Paleoproterozoic snowball Earth: A climate disaster triggered by the evolution of oxygenic photosynthesis. *Proc. Natl. Acad. Sci. U.S.A.* **102**, 11131–11136 (2005).
5. S. J. Wang, R. L. Rudnick, R. M. Gaschnig, H. Wang, L. E. Wasylenki, Methanogenesis sustained by sulfide weathering during the great oxidation event. *Nat. Geosci.* **12**, 296–300 (2019).
6. T. A. Laakso, D. P. Schrag, Methane in the precambrian atmosphere. *Earth Planet. Sci. Lett.* **522**, 48–54 (2019).
7. M. W. Claire, D. C. Catling, K. J. Zahnle, Biogeochemical modelling of the rise in atmospheric oxygen. *Geobiology* **4**, 239–269 (2006).
8. H. D. Holland, Why the atmosphere became oxygenated: A proposal. *Geochim. Cosmochim. Acta* **73**, 5241–5255 (2009).
9. J. L. Kirschvink *et al*., Paleoproterozoic snowball earth: Extreme climatic and geochemical global change and its biological consequences. *Proc. Natl. Acad. Sci. U.S.A.* **97**, 1400–1405 (2000).
10. T. A. Laakso, D. P. Schrag, A theory of atmospheric oxygen. *Geobiology* **15**, 366–384 (2017).
11. C. T. Reinhard, N. J. Planavsky, T. W. Lyons, Long-term sedimentary recycling of rare sulphur isotope anomalies. *Nature* **497**, 100–103 (2013).
12. J. Farquhar, B. A. Wing, Multiple sulfur isotopes and the evolution of the atmosphere. *Earth Planet. Sci. Lett.* **213**, 1–13 (2003).
13. P. Philippot *et al*., Globally asynchronous sulphur isotope signals require re-definition of the Great Oxidation Event. *Nat. Commun.* **9**, 2245 (2018).
14. P. F. Hoffman, The great oxidation and a Siderian snowball Earth: MIF-S based correlation of Paleoproterozoic glacial epochs. *Chem. Geol.* **362**, 143–156 (2013).
15. B. A. Killingsworth *et al*., Constraining the rise of oxygen with oxygen isotopes. *Nat. Commun.* **10**, 4924 (2019).
16. A. P. Gumsley *et al*., Timing and tempo of the great oxidation event. *Proc. Natl. Acad. Sci. U.S.A.* **114**, 1811–1816 (2017).
17. V. A. Melezhik *et al*., "6.1 The imandra/varzuga Greenstone Belt" in *Reading the Archive of Earth's Oxygenation*, V. A. Melezhik, Ed. (Springer, 2013), Vol. 2, pp. 505–590.
18. S. Soomer *et al*., High-CO 2, acidic and oxygen-starved weathering at the Fennoscandian Shield at the Archean-Proterozoic transition. *Precambrian Res.* **327**, 68–80 (2019).
19. A. T. Brasier *et al*., Earth's earliest global glaciation? Carbonate geochemistry and geochronology of the Polisarka Sedimentary formation, Kola Peninsula, Russia. *Precambrian Res.* **235**, 278–294 (2013).
20. Y. V. Amelin, L. M. Heaman, V. S. Semenov, UPb geochronology of layered mafic intrusions in the eastern Baltic Shield: Implications for the timing and duration of Paleoproterozoic continental rifting. *Precambrian Res.* **75**, 31–46 (1995).
21. V. V. Chashchin, T. B. Bayanova, N. V. Levkovich, Volcanoplutonic association of the early-stage evolution of the Imandra-Varzuga rift zone, Kola Peninsula, Russia: Geological, petrogeochemical, and isotope-geochronological data. *Petrology* **16**, 279–298 (2008).
22. A. B. Vrevskii, E. S. Bogomolov, T. F. Zinger, S. A. Sergeev, Polychronic sources and isotopic age of the volcanogenic complex (Arvarench Unit) of the Imandra-Varzuga structure, Kola Peninsula. *Dokl. Earth Sci.* **431**, 386–389 (2010).
23. S. Ono, Photochemistry of sulfur dioxide and the origin of mass-independent isotope fractionation in Earth's atmosphere. *Annu. Rev. Earth Planet. Sci.* **45**, 301–329 (2017).
24. J. Farquhar, D. T. Johnston, B. A. Wing, Implications of conservation of mass effects on mass-dependent isotope fractionations: Influence of network structure on sulfur isotope phase space of dissimilatory sulfate reduction. *Geochim. Cosmochim. Acta* **71**, 5862–5875 (2007).
25. J. Farquhar *et al*., Isotopic evidence for Mesoarchaean anoxia and changing atmospheric sulphur chemistry. *Nature* **449**, 706–709 (2007).
26. S. Ono *et al*., New insights into Archean sulfur cycle from mass-independent sulfur isotope records from the Hamersley Basin, Australia. *Earth Planet. Sci. Lett.* **213**, 15–30 (2003).
27. S. Ono, A. J. Kaufman, J. Farquhar, D. Y. Sumner, N. J. Beukes, Lithofacies control on multiple-sulfur isotope records and Neoarchean sulfur cycles. *Precambrian Res.* **169**, 58–67 (2009).
28. A. L. Zerkle, M. W. Claire, S. D. Domagal-Goldman, J. Farquhar, S. W. Poulton, A bistable organic-rich atmosphere on the Neoarchaean Earth. *Nat. Geosci.* **5**, 359–363 (2012).
29. G. Izon *et al*., Multiple oscillations in Neoarchaean atmospheric chemistry. *Earth Planet. Sci. Lett.* **431**, 264–273 (2015).
30. G. Izon *et al*., Biological regulation of atmospheric chemistry en route to planetary oxygenation. *Proc. Natl. Acad. Sci. U.S.A.* **114**, E2571–E2579 (2017).
31. B. Rasmussen, A. Bekker, I. R. Fletcher, Correlation of Paleoproterozoic glaciations based on U-Pb zircon ages for tuff beds in the Transvaal and Huronian Supergroups. *Earth Planet. Sci. Lett.* **382**, 173–180 (2013).
32. A. P. Martin, D. J. Condon, A. R. Prave, A. Lepland, A review of temporal constraints for the Palaeoproterozoic large, positive carbonate carbon isotope excursion (the Lomagundi-Jatuli Event). *Earth Sci. Rev.* **127**, 242–261 (2013).
33. T. Caquineau, J. L. Paquette, P. Philippot, U-Pb detrital zircon geochronology of the Turee Creek group, Hamersley Basin, Western Australia: Timing and correlation of the Paleoproterozoic glaciations. *Precambrian Res.* **307**, 34–50 (2018).
34. Q. Guo *et al*., Reconstructing Earth's surface oxidation across the Archean-Proterozoic transition. *Geology* **37**, 399–402 (2009).
35. G. Luo *et al*., Rapid oxygenation of Earth's atmosphere 2.33 billion years ago. *Sci. Adv.* **2**, e1600134 (2016).
36. M. R. Warke, S. Schröder, Synsedimentary fault control on the deposition of the Duitschland Formation (South Africa): Implications for depositional settings, Paleoproterozoic stratigraphic correlations, and the GOE. *Precambrian Res.* **310**, 348–364 (2018).
37. D. R. Nelson, A. F. Trendall, W. Altermann, Chronological correlations between the Pilbara and Kaapvaal cratons. *Precambrian Res.* **97**, 165–189 (1999).
38. S. Schröder, N. J. Beukes, R. A. Armstrong, Detrital zircon constraints on the tectonostratigraphy of the Paleoproterozoic Pretoria group, South Africa. *Precambrian Res.* **278**, 362–393 (2016).
39. J. L. Hannah, A. Bekker, H. J. Stein, R. J. Markey, H. D. Holland, Primitive Os and 2316 Ma age for marine shale: Implications for Paleoproterozoic glacial events and the rise of atmospheric oxygen. *Earth Planet. Sci. Lett.* **225**, 43–52 (2004).
40. M. Bau, R. L. Romer, V. Lüders, N. J. Beukes, Pb, O, and C isotopes in silicified Mooidraai dolomite (Transvaal Supergroup, South Africa): Implications for the composition of Paleoproterozoic seawater and "dating" the increase of oxygen in the Precambrian atmosphere. *Earth Planet. Sci. Lett.* **174**, 43–57 (1999).
41. B. Fairey, H. Tsikos, F. Corfu, S. Polteau, U-Pb systematics in carbonates of the Postmasburg group, transvaal Supergroup, South Africa: Primary versus metasomatic controls. *Precambrian Res.* **231**, 194–205 (2013).
42. E. D. Swanner *et al*., Geochemistry of pyrite from diamictites of the Boolgeeda Iron Formation, Western Australia with implications for the GOE and Paleoproterozoic ice ages. *Chem. Geol.* **362**, 131–142 (2013).
43. R. C. Martindale *et al*., Sedimentology, chemostratigraphy, and stromatolites of lower Paleoproterozoic carbonates, Turee Creek group, Western Australia. *Precambrian Res.* **266**, 194–211 (2015).
44. D. Papineau, S. J. Mojzsis, A. K. Schmitt, Multiple sulfur isotopes from Paleoproterozoic Huronian interglacial sediments and the rise of atmospheric oxygen. *Earth Planet. Sci. Lett.* **255**, 188–212 (2007).
45. K. Y. Ketchum, L. M. Heaman, G. Bennett, D. J. Hughes, Age, petrogenesis and tectonic setting of the Thessalon volcanic rocks, Huronian Supergroup, Canada. *Precambrian Res.* **233**, 144–172 (2013).
46. H. Cui *et al*., Searching for the great oxidation event in North America: A reappraisal of the huronian Supergroup by SIMS sulfur four-isotope analysis. *Astrobiology* **18**, 519–538 (2018).
47. T. C. Kampmann, A. P. Gumsley, M. O. de Kock, U. Söderlund, U-Pb geochronology and paleomagnetism of the Westerberg Sill suite, Kaapvaal Craton - support for a coherent Kaapvaal-Pilbara block (Vaalbara) into the Paleoproterozoic? *Precambrian Res.* **269**, 58–72 (2015).
48. J. Farquhar, A. L. Zerkle, A. Bekker, "Geologic and geochemical constraints on earth's early atmosphere" in *Treatise on Geochemistry*, H. D. Holland, K. K. Turekian, Eds. (Elsevier Ltd., ed. 2, 2014), pp. 91–138.
49. D. C. Catling, K. J. Zahnle, The Archean atmosphere. *Sci. Adv.* **6**, eaax1420 (2020).
50. K. Zahnle, M. Claire, D. Catling, The loss of mass-independent fractionation in sulfur due to a Palaeoproterozoic collapse of atmospheric methane. *Geobiology* **4**, 271–283 (2006).
51. G. Avice *et al*., Evolution of atmospheric xenon and other noble gases inferred from Archean to Paleoproterozoic rocks. *Geochim. Cosmochim. Acta* **232**, 82–100 (2018).
52. A. Lepland *et al*., "5.1 FAR-DEEP core archive and database" in *Reading the Archive of Earth's Oxygenation*, V. A. Melezhik, Ed. (Springer, 2013), Vol. 2, pp. 493–502.
53. Y. Ueno, S. Aoyama, Y. Endo, F. Matsu'ura, J. Foriel, Rapid quadruple sulfur isotope analysis at the sub-micromole level by a flash heating with CoF 3. *Chem. Geol.* **419**, 29–35 (2015).
54. M. R. Warke *et al*, The Great Oxidation Event preceded a Paleoproterozoic snowball Earth (dataset). St Andrews Research Portal. https://doi.org/10.17630/2faeb51f-7353-4fbc-abdd-cbc7991cf44b. Deposited 14 April 2020.